Science of Sintering, **55** (2023) 453-467

https://doi.org/10.2298/SOS220715018M

UDK: 666.3.019; 663.442; 675.017.5

Influence of Mechanochemical Activation on the Thermal Behavior of Pyrophyllite

Andjela Mitrović Rajić[1], Tijana Pantić[1], Sanja Milošević Govedarović[1], Bojana Paskaš Mamula[1], Nenad Filipović[2], Jasmina Grbović Novaković[1*)], Silvana Dimitrijević[3]

[1]Centre of Excellence for Hydrogen and Renewable Energy, Laboratory of Physics, Vinča Institute of Nuclear Sciences - National Institute of Republic of Serbia, University of Belgrade, Belgrade, Serbia

[2]Institute of Technical Sciences of SASA, Kneza Mihaila 35/IV, 11000 Belgrade, Serbia

[3]The Mining and Metallurgy Institute Bor, Zeleni Bulevar 35, 1210 Bor

Abstract:

The effect of mechanical milling on the thermal behavior of pyrophyllite ore from a deposit in Parsovići, Bosnia and Herzegovina, was characterized by X-ray powder diffraction, Fourier transform infrared spectroscopy, scanning electron microscopy, and Particle size distribution. The thermal behavior of the material was followed by thermogravimetric and differential thermal analysis and correlated to its microstructural properties. The Williamson-Hall model was used to calculate the crystallite size and microstrain. Mechanochemical treatment of pyrophyllite ore produced a substantial structural modification, mainly along the c axis, resulting in disorder and partial degradation of the crystal structure of the ore. The particle size diminution, induced defects, and microstrain in the crystal lattice cause decrease in the peak intensity until the final disappearance. As confirmed by scanning electron microscopy and particle-size-distribution analysis, the surface area and the agglomeration is more pronounced as grinding time increases. Dehydroxylation of the minerals in the unmilled ore was realized at 716^{o}C confirm by FTIR analysis. The endothermic peak that corresponds to dehydroxylation is shifted toward lower temperatures and becomes broad giving rise to the formation of amorphous SiO_2 as milling time increases.

Keywords*: Thermal behavior; Ceramics; Pyrophyllite clay; Mechanochemistry; Mechanical milling.*

1. Introduction

Pyrophyllite is a phyllosilicate mineral composed of aluminum silicate hydroxide of the chemical formula $Al_2Si_4O_{10}(OH)_2$ [1-4]. The crystal lattice of pyrophyllite consists of an octahedral sheet of $AlO_4(OH)_2$ located between two SiO_4 tetrahedral layers. Thus, pyrophyllite has a 2:1 layered structure, while the bonds between layers are weak van der Walls, so the layers can easily slide over each other [1-12]. As was explained by Dixon et al.[13] pyrophyllite shows either the absence of negative charge in the layers or it is

*) **Corresponding author:** jasnag@vin.bg.ac.rs

negligibly small giving rise to unique physicochemical characteristics such as low thermal and electrical conductivity, high melting point, low expansion coefficient, low reversible thermal expansion, and excellent reheating stability[1-13]. Similar to other clays, it is used in porcelain, building materials, fire-resistant material, insecticide, textiles, detergents, cosmetics, and as the filler for rubberizing, papermaking, painting, etc [6, 14-20]. Different applications of pyrophyllite starting from heavy metal and organic pollutant adsorbents to various types of ceramics including refractories, enamels, and ceramics membranes, require different modifications methods [1-22]:

1. adsorption;
2. ion exchange with inorganic cations and cationic complex;
3. ion exchange with organic cations;
4. binding of inorganic and organic anions, mainly at the edges;
5. grafting of organic compounds;
6. reaction with acids;
7. pillaring by different types of poly- (hydroxo metal) cation;
8. interlamellar or intraparticle and interparticle polymerization;
9. dehydroxylation and calcination;
10. delamination and reaggregation of smectitic clay minerals;
11. physical treatments such as lyophilization, ultrasound, and plasma.

Mechanochemical activation (MCA) is an environmentally friendly green chemistry method because it avoids the use of solvents [4]. The MCA process introduces structural disorder, accordingly reducing particle size and causing amorphization and an increase in the chemical reactivity of material [23, 24]. It has been shown that, in contrast to the high chemical stability of pyrophyllite, the MCA of pyrophyllite and its ores results in noteworthy structural distortion and reduction of particles and crystallite size [3-9, 11-13, 25-29]. Zhang et al. [3] studied pyrophyllite from Zhejiang province, located in the southeastern region of China. They proved that pyrophyllite from this area was resistant to mechanical destruction and the crystalline order of pyrophyllite was not destroyed until milling for 240 min with the ball-to-powder ratio of 20:1. Wiewióra et al. [29] worked on mechanical activation on pyrophyllite from Zalamea (Badajoz, Spain). The natural sample was a mixture of pyrophyllite, kaolinite, mixed layer illite-smectite, and illite. A small content of rutile and quartz shows that amorphous aggregates of pyrophyllite containing quartz have been developed after grinding. Applying mechanical milling improves the sorption activity of pyrophyllite samples in the size range of 0.1–2.5 μm, Mohammadnejad et al. [6] concluded that the pyrophyllite particles undergo chemical as well as structural changes which influence the rate of surface activation and consequently the extent of gold absorption. Perez-Rodriguez et al.[7] investigated the effect of milling on pyrophyllite from Hillsboro (North Carolina, USA). In this case, the natural sample was a mixture of pyrophyllite, mica, and kaolinite. They showed that high-energy mechanical milling leads to distortion of the crystal structure, reduction in particle size, and aggregation. Kim et al. [30] worked with ore of pyrophyllite from the Wando mine (Haenam, South Korea) and found that this ore of pyrophyllite consists of pyrophyllite, diaspore, kaolinite, rutile, and dickite Erdemoğlu et al. [31] investigated pyrophyllite deposits mined in the Pütürge region (Malatya, Turkey). This deposit besides pyrophyllite contains muscovite, quartz, kaolinite, muscovite, topaz, and diaspora. They concluded that intensive milling affects X-ray diffraction peak intensities of pyrophyllite, muscovite, and kaolinite, except quartz. In this study, we have investigated the influence of high-energy ball milling of pyrophyllite from Parsovići mine, Bosnia and Herzegovina, supplied by AD HARBI, Sarajevo on the thermal behavior of samples with the final aim to develop the low-cost material for ceramic membranes.

2. Materials and Experimental Procedures

Mechanical milling of pyrophyllite ore was done in a SPEX Mixer mill 5100 using different milling times, as listed in Table I, using a standard procedure (20 min. milling, 20 minutes resting) to avoid overheating of samples. The mass of the ball was 1 g. The ball-to-powder ratio (BPR) was 10:1. Table I shows the denomination and milling time of samples of pyrophyllite.

Tab. I Sample denomination and milling time of pyrophyllite.

Sample label	Milling time (min)
P-0	0
P-5	5
P-10	10
P-15	15
P-20	20
P-30	30
P-60	60
P-120	120

The phase composition of samples was examined by X-ray diffraction (Rigaku Ultima IV, Japan) operating at 40 kV and 40 mA using nickel-filtered CuKα1 radiation (λ = 0.1540 nm). XRD data were collected in (2θ) range 5 to 80° in steps of 0.02° for 10 s. Phase analysis was done by using the PDXL2 software (version 2.0.3.0, 2011, Rigaku Corporation, Tokyo, Japan), with the reference to the patterns of the International Centre for Diffraction Database (ICDD), version 2012.

Crystallite size and lattice strain are calculated using XRD profile analysis using the Williamson-Hall plot according to Eq. (1) [32]:

$$\beta\cos(\theta) = 2\varepsilon\sin(\theta) + \frac{0.9\lambda}{D} \qquad (1)$$

where k = 0.9 is the shape factor and β is the corrected peak full width at half maximum (FWHM) [33].

The $\beta\cos(\theta)$ is plotted as a function of $\sin(\theta)$ and a straight line is derived using the least squares method with an intercept at 0.9 λ/D and a slope of 2ε. Both crystallite size D and lattice strain ε are calculated from Equation (1).

The qualitative analysis of the samples was performed on Thermo Scientific Nicolet iS10 Spectrometer using the attenuated total reflectance (ATR) sampling technique. FTIR spectra were recorded in the range of 400–4000 cm^{-1} and expressed as an average of 32 scans. The spectral resolution was 4 cm^{-1}.

The resulting modifications and phase distribution of the mechanochemically activated clay samples, as well as material homogeneity and morphology of the powder particles, were investigated by scanning electron microscopy (SEM) using JEOL JSM6610LV. Energy-dispersive spectroscopy (EDS) was used for the surface elemental analysis. The micrographs were taken on as-received samples without preparation (micrographs marked with (a) on the SEM image) as well as on samples prepared by standard metallographic procedure (micrographs marked with (b) on the SEM image).

A Malvern 2000SM Mastersizer laser scattering particle size analyzer has been used to obtain the particle size distribution of samples. The specified resolution range of the system was sub-μm to 2 mm. 2-propanol was used as suspension media. All samples were ultrasonicated for 10 min before measurement. All measurements were performed at the same stirring speed and obscuration level.

Simultaneous thermal analysis of samples was performed on SETARAM apparatus (Setsys Evolution) for thermal gravimetric and differential thermal analysis (TGA-DTA). Powder samples form were placed in alumina crucibles and heated up to 1000°C, with a heating rate of 10 °C/min. The working atmosphere was synthetic air.

3. Results and Discussion

As shown in Fig. 1, XRD patterns of pyrophyllite ore from the Parsovići mine, Bosnia and Herzegovina contain pyrophyllite, quartz, kaolinite, calcite, and muscovite, unlike other deposits.[3, 6, 7, 29-31]. The X-ray diffraction patterns of pyrophyllite ore, before and after milling for different milling times, are shown in Fig. 2. Two major phases found in the ore are *pyrophyllite* with characteristic reflections at 2θ 9.68, 29.21, and quartz with reflections at 2θ 20.85, 26.72 [3]. Mechanical milling produced a significant structural modification, resulting in increased amorphization.

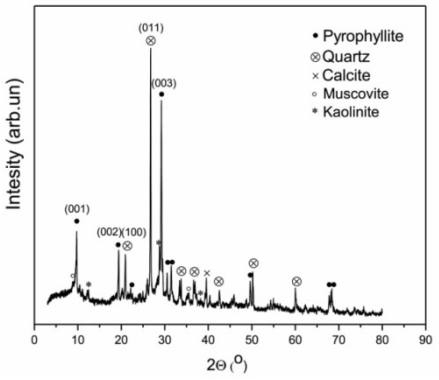

Fig. 1. XRD patterns of pyrophyllite ore from the Parsovići mine, Bosnia and Herzegovina.

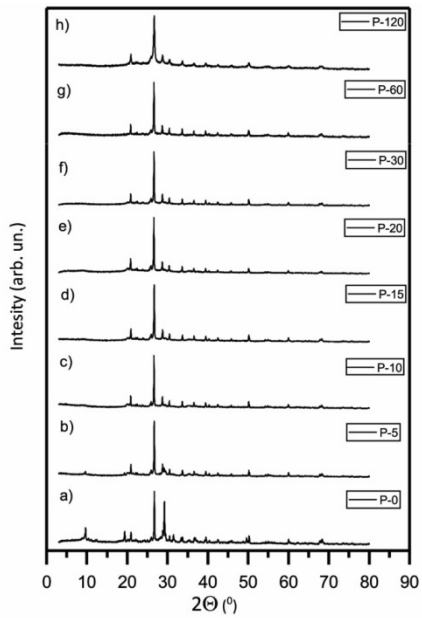

Fig. 2. XRD analysis before and after milling for different times of pyrophyllite ore from Parsovići mine, Bosnia and Herzegovina: a) 0 min; b) 5 min; c) 10 min; d) 15 min; e) 20 min; f) 30 min; g) 60 min; h) 120 min.

Tab. II Comparison of typical d values for pyrophyllite and quartz from different mines.

References	$d_{pyrophyllite}$ (Å) (001)	$d_{pyrophyllite}$ (Å) (003)	d_{quartz} (Å) (100)	d_{quartz} (Å) (011)
Zhang et al.[3]	9.25	3.07	4.26	3.35
Bentayeb et al.[34]	9.20	3.06	4.26	3.34
Erdemoğlu et al.[31]	9.26	3.03	358	3.35
This work	9.13	3.05	4.24	3.31

This is evidenced by a progressive decrease in the typical XRD reflection intensities with prolonged time of milling (Fig. 2). The broadening of typical maxima of *pyrophyllite* is also observed. After 30 min of mechanical milling, the reflections (001), (002), (003), and (005) of pyrophyllite almost disappear, while amorphization occurs after 120 min. Similar behavior was observed using ore from different mines [6-8]. Broadening of typical peaks and decreasing of X-ray intensities originated mainly from particle size reduction, as can be seen in Table II, as well as induced stress and strain into a lattice (Table III). Our results confirm previous findings by other authors: the largest structural disorder occurs mainly along the c-axis of crystal (stacking direction for tetrahedral and octahedral sheets which are connected through weak H-bonding/Van der Waals bonding) even though (003) reflections do not disappear completely upon milling [6-8].

Tab. III Crystallite, particle size, the geometrical specific surface area of samples of pyrophyllite ore milled for different milling times: a) 0 min; b) 5min; c) 10 min; d) 15 min; e) 20 min; f) 30 min; g) 60 min; h) 120 min.

Sample	**Specific area (m^2/g)**	**Particle size d (0,5) (μm)**	**Crystallite size $D_{pyrophyllite}$ (nm)**	**Strain $\varepsilon_{pyrophyllite}$**	**Crystallite size D_{quartz} (nm)**	**ε_{quartz}**
P-0	0.04	172	10	0.0080	115	0.0003
P-5	1.54	6.02	12	0.0092	22	0.0039
P-10	1.71	5.70	10	0.0088	15	0.0026
P-15	1.89	5.57	10	0.0080	19	0.0021
P-20	1.82	5.94	72	0.0030	57	0.0013
P-30	1.74	6.41	10	0.0079	22	0.0038
P-60	1.82	7.19	17	0.0023	46	0.0016
P-120	1.95	7.54	27	0.0050	71	0.0002

To shed more light on the structural modification and type of chemical change during mechanical milling, FTIR analysis is carried out.

FTIR spectra and assignment of each band of milled and unmilled samples are shown in Fig. 3 and Table IV, respectively. Different bands appear depending on the milling time, confirming the structural disorder observed by XRD. The unmilled sample (P-0) showed a strong band at 3672 cm^{-1} which can be assigned to OH vibration from Al-OH linkage [3]. At 1120 cm^{-1}, a strong band is observed that can be attributed to Si-O stretching vibration.

The bands at 832 cm^{-1} and 943 cm^{-1} correspond to Al-OH bending vibration. The peak at 518 cm^{-1} can be assigned to Si-O-Si bending vibration. The vibration at 1616 cm^{-1} corresponds to bending the OH surface group [3]. The band at 802 cm^{-1} corresponds to the characteristic bands of silica [35]. The band at 754 cm^{-1} indicates the presence of Si–O–Al where Al is in tetrahedral coordination. It also indicates that there is a possible presence of sericite/muscovite minerals. The peak at 532 cm^{-1} can be assigned to octahedral AlO_6 sheet

vibrations. The band at 1028 cm^{-1} can be assigned to the intense Si–O and Si–O–Al stretching vibrations, characteristic of aluminosilicates [14]. The band at 450 cm^{-1} corresponds to the bending of Si – O groups.[36] After 5 min of grinding, the bands at 779 cm^{-1} and 797 cm^{-1} appear indicating the presence of quartz and thus confirming the results of XRD analysis [3].

Tab. IV FTIR vibration band positions and their assignments for pyrophyllite ore from Parsovići mine, Bosnia and Herzegovina, before and after milling for different times: a) 0 min; b) 5 min; c) 10 min d) 15 min; e) 20 min; f) 30 min; g) 60 min; h) 120 min.

Wavenumbers (cm^{-1})								
P-0	P-5	P-10	P-15	P-20	P-30	P-60	P-120	Vibrations
-	414	416	-	-	-	-	-	
450	443 448	438	449	451	447	450	450	Bending of Si – O groups
-	-	478	-	-	-	-	-	Octahedral AlO6 sheet vibrations
518	517	519	511	516	511	509	516	Si-O-Si bending vibration
532	534	532	534	539	-	-	-	Octahedral AlO6 sheet vibrations
694	693	696	693	694	698	692	693	Presence of quartz
754	-	-	-	-	-	-	-	The presence of Si–O-Al where Al is in tetrahedral coordination supports the earlier observation of the possible presence of muscovite minerals.
-	777	776	779	778	776	779	777	Presence of quartz
-	799	795	796	797	797	797	797	
802	-	-	-	-	-	-	-	The characteristic bands of silica
832	835	-	-	-	-	-	-	Al-OH bending vibration
-	869	-	882	878	881	879	-	Al-OH bending vibration
943	943	943	-	-	-	-	-	Al-OH bending vibration
-	-	-	950	945	-	-	-	Al–(OH) vibration
-	-	987	-	-	-	-	-	
1009	-	-	-	-	-	-	-	
1028	1022	-	-	-	-	-	-	The intense Si–O and Si–O–Al stretching frequencies, characteristic of aluminosilicates
-	-	1049	1048	1052	1045	1051	1058	Si-O-Si linkage, characteristic peaks of aluminosilicates.
1120	1120	1119	-	-	-	-	-	Si-O stretching vibrations
-	-	1159	-	-	-	-	-	
-	1425	-	-	-	-	-	-	
-	-	1439	1442	1448	1450	-		Si-O-Si bending vibration
1616	1589	-	-	-	-	-	-	Bending the OH surface group
-	3290	-	-	-	-	-	-	OH stretching of the surface water
3672	3672	3674	3671	3666	3674	-	-	OH vibration of the Al OH linkage

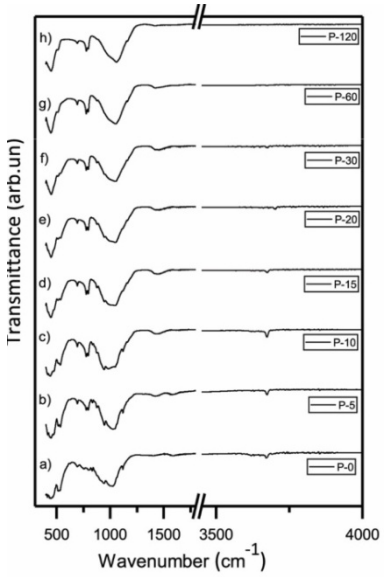

Fig. 3. FTIR spectra before and after milling for different times of pyrophyllite ore from Parsovići mine, Bosnia and Herzegovina: a) 0 min; b) 5min; c) 10 min; d) 15 min; e) 20 min; f) 30 min; g) 60 min; h) 120 min.

These vibrations are present even after 120 min of grinding, indicating that quartz has a more stable structure than pyrophyllite [11]. After 15 min of grinding, the vibration at 1120 cm^{-1} disappears indicating a breakdown of the Si-O band, which means that the tetrahedral sheets have been destroyed. Also, after 60 minutes of milling, the bands at 3673 cm^{-1}, 943 cm^{-1}, and 832 cm^{-1} disappeared, as a result of the release of OH groups from the Al-centered octahedrons. Therefore, the octahedral sheets are damaged [3]. The intensity of the band at 518 cm^{-1} decreases with increasing milling time as a consequence of the collapse of the Si-O-Al band, resulting in a broken link between the tetrahedral and octahedral sheets [3].

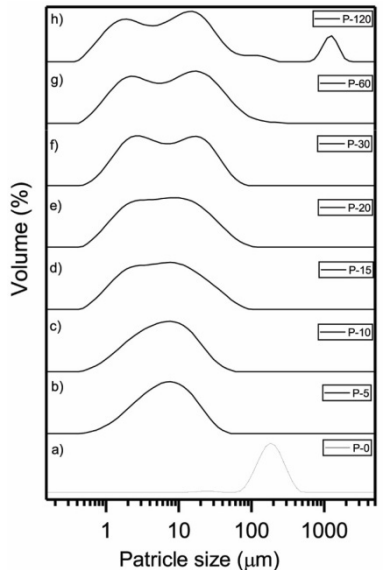

Fig. 4. Particle size distribution of pyrophyllite ore from Parsovići mine, Bosnia and Herzegovina before and after milling for different times: a) 0 min; b) 5 min; c) 10 min; d) 15 min; e) 20 min; f) 30 min; g) 60 min; h) 120 min.

Tab.V Particle size and the fraction of particles for samples ball milled between 15 and 60 min were obtained by PSD analysis.

Sample	Particle size (μm)	Fraction (%)
P-15	3	30
	8	70
P-20	3	37
	10	63
P-30	3	53
	17	47
P-60	2	40
	17	60

Fig. 4. shows the particle size distribution for all samples. Monomodal symmetric particle size distribution is observed for as-received sample P-0 with a maximum of 172 μm. Short mechanical milling up to 10 min preserved monomodal asymmetric particle size distribution, as shown in Fig. 4b-c, with maxima ranging from 5-6 μm. Bimodal particle size distribution is observed for samples milled from 15-60 min. The sample milled for 120 min show polymodal distribution with an increased number of particles, with sizes over 1000 μm due to pronounced agglomeration [37-39]. The particle size and fraction of particles having bimodal particle size distribution have been summarized in Table V. An increase in the fraction of smaller particles is observed.

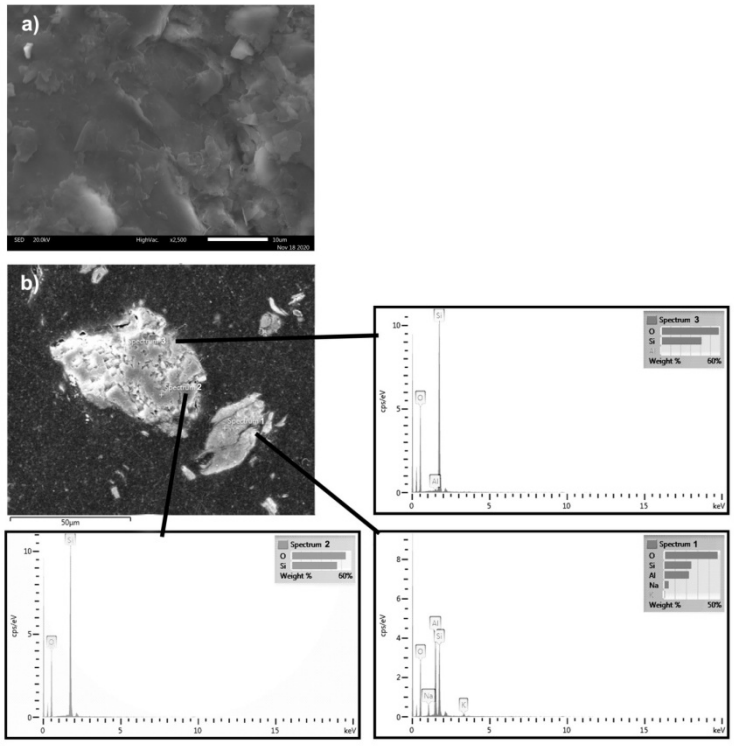

Fig. 5a. SEM-EDS micrographs of pyrophyllite ore from mine Parsovići mine, Bosnia and Herzegovina: a) before (P0) and b) after 10 min of milling (P-10). SEM micrograph (a) is obtained on the sample without metallographic preparation; SEM micrograph (b) is obtained on a sample with metallographic preparation.

The size reduction and associated morphological changes which occur during the milling of pyrophyllite are examined by SEM-EDS analysis. The selected micrographs are shown in Fig. 5. The particles of as-received sample P0 show rough surfaces, and the sizes are not uniform, with single particles showing a laminar structure (Fig. 5a). EDS analysis strongly indicates the presence of SiO_2 (particles with sharp edges), *pyrophyllite*, kaolinite, calcite, and muscovite in the ore [37-39]. When milling begins, the particle size decreases (see SEM micrograph in Fig. 5b). When the milling time is long, quasi-spherical aggregates are produced [3, 9].

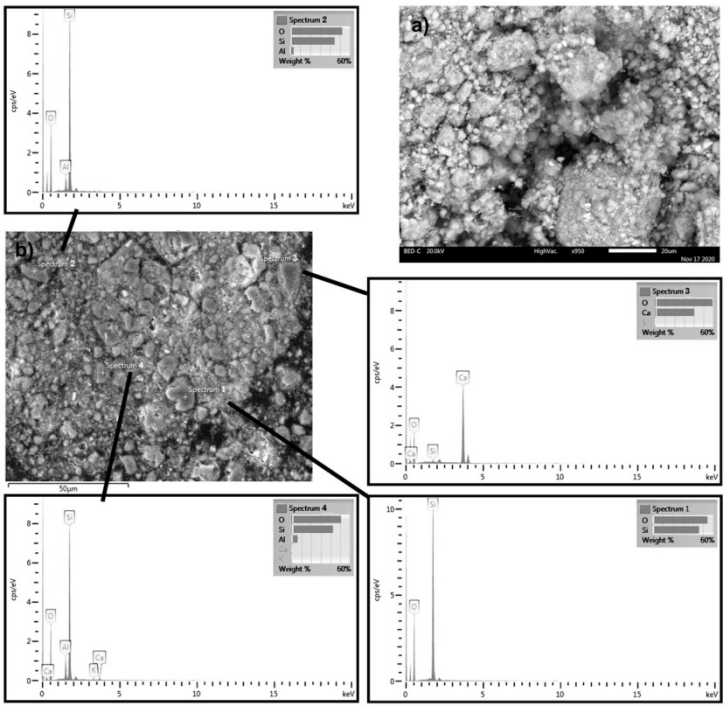

Fig. 5b. SEM-EDS micrographs of pyrophyllite ore from mine Parsovići mine, Bosnia and Herzegovina: a) before (P0) and b) after 10 min of milling (P-10). SEM micrograph (a) is obtained on the sample without metallographic preparation; SEM micrograph (b) is obtained on a sample with metallographic preparation.

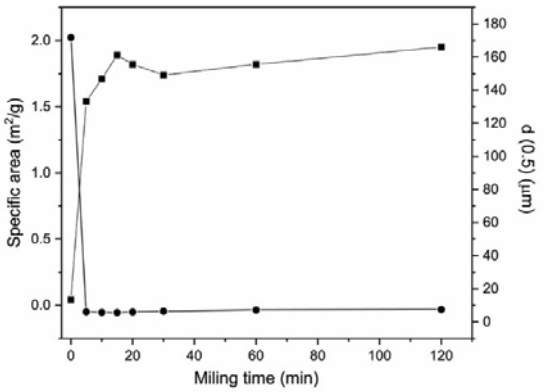

Fig. 6. Geometric specific surface area and particle size d (0.5) before and after milling for different times from 0-120 min of pyrophyllite ore from Parsovići mine, Bosnia and Herzegovina.

As it was explained by Pérez-Rodríguez et al.[7] at the beginning of grinding, the destruction of the layers in the pyrophyllite structure takes place until the particle size decreases. As can be seen from Fig. 6 and Table III, these processes lead to an increase in the geometrical specific surface area. However, long milling time leads to the formation of agglomerates and the geometric specific surface area begins to decrease. The particles gradually lose their original layered shape and become rounded-edge particles with a rugged surface. At longer grinding times, the agglomerates are constituted by a greater number of welded particles. Further, mechanical milling causes a noteworthy number of micropores.

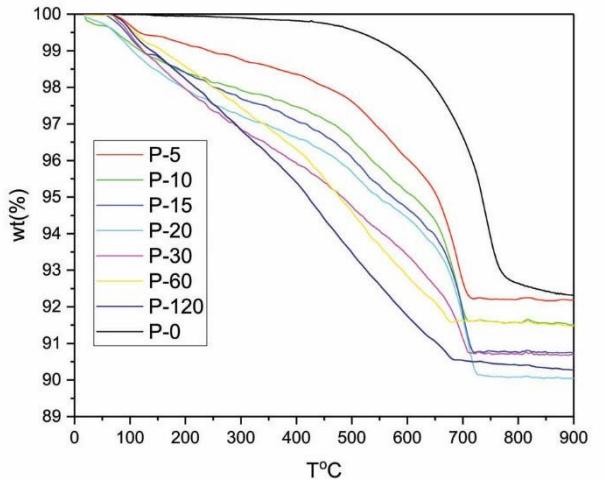

Fig. 7. TG diagrams before and after milling for different times of pyrophyllite ore from Parsovići mine, Bosnia and Herzegovina: P-0) 0 min; P-5) 5 min; P-10) 10 min; P-15) 15 min; P-20) 20 min; P-30) 30 min; P-60) 60 min; P-120) 120 min.

Tab. VI Weight loss, peak range, and peak maximum before and after milling for different milling times of pyrophyllite ore from Parsovići, Bosnia and Herzegovina: (P-0) 0 min; (P-5) 5 min; (P-10) 10 min; (P-15) 15 min; (P-20) 20 min; (P-30) 30 min; (P-60) 60 min; (P-120) 120 min.

Sample	TG	DTA	
	Weight loss Δm (%)	Peak range (°C)	Peak maximum (°C)
P-0	5.500	580-750	716
P-5	7.845	640-720	702
P-10	8.563	600-720	695
P-15	9.247	630-740	712
P-20	10.008	640-740	718
P-30	9.307	660-720	705
P-60	8.503	630-700	672
P-120	9.766	630-700	676

The existence of a milling limit is determined mainly by the tendency of the particles to agglomerate (see Fig. 6). The milling limit of a pyrophyllite ore depends on its composition and the impurities that enter into its composition and in the case of ore from the Parsovići mine is 20 min [11]. EDX spectra before and after mechanochemical treatment of

pyrophyllite ore show silicon and aluminum as major elements and small amounts of magnesium, potassium, sodium, calcium, and iron which corresponds to the chemical composition of the Parsovići mine. Mechanical grinding causes dealumination; hence as silicon content continued to increase correspondently with longer milling time, the aluminum content decreases [40].

Tab. VII The thermal transformation takes place during the heating of different minerals and pyrophyllite ore from the Parsovići mine, Bosnia and Herzegovina.

Mineral	Temperature range	Thermal transformation phase	Ref.
Pyrophyllite	<450℃	Removal of the surface, pore, and adsorbed water	[2]
	780℃<T <1100℃	Dehydroxylation	[44]
	780℃<T <1100℃	Formation of amorphous SiO_2	[45]
	T>1200℃	Formation of mullite and crystallization of cristobalite from amorphous SiO_2	[46] [15]
Pyrophyllite	<500℃	Dehydroxylation	[43]
	700℃<T <800℃	Maximum structural water loss	[47]
	T=1050℃	Water is eliminated	[2]
	T=1215℃	Mullite crystallization with a simultaneous	[48]
	T=1325℃	disappearance of pyrophyllite dehydroxylate.	[49]
	T=1430℃	Cristobalite crystallization.	[50]
		Mullite and cristobalite phases are well crystallized	[43]
Kaolinite	<400℃	Removal of the surface, pore, and adsorbed water	[51]
	400℃<T <700℃	Dehydroxylation	
	T =∼1000	Formation of mullite phase and amorphous SiO2	
	T>1200℃	Crystallization of cristobalite from amorphous SiO_2	
Muscovite	T<350℃	Removal of the surface, pore, and adsorbed water	[52]
	475℃<T <950℃	Dehydroxylation	[53]
	T =∼1050℃	Formation of spinel ($MgAl_2O_4$) and sanidine ($KAlSi_3O_8$)	[54]
	T>1300℃	Formation of mullite and leucite phases ($KAlSi_2O_6$)	[55]
Pyrophillite Parsovići	600℃<T <800℃	Dehydroxylation and maximum of structural water removed	This work

Thermogravimetric (TG) analysis is shown in Fig. 7 for both as-received and mechanochemically modified samples. As it can be noticed, the weight loss for the as-received sample begins at about 550^{o}C and ends at about 750^{o}C after the TG curve reaches the plateau. The total weight loss agrees with the calculated value for ideal pyrophyllite within 5% [41, 42]. According to Rodriguez et al., weight loss can be attributed to the loss of water by dehydroxylation [25]. As can be seen from Table VI, the weight loss gradually increases to 10% for the sample milled for 20 min. This can be attributed to phase transformations of other constituents as noticed by FTIR analysis. The long mechanochemical treatment causes a decrease in weight loss and can be attributed to the agglomeration of particles. Table VII. summarizes the literature data related to different processes that occur during heating. One could speculate that some increase in weight in the as-received sample is due to adsorbed species at the surface of the sample.

The reaction of dehydroxylation and structure decomposition takes place between 450 and 850°C according to the:

$$3Al_2Si_4O_{10}(OH)_2 = 3Al_2O_3{\cdot}2SiO_2 \text{ (mullite)} + 10SiO_2 \text{ (cristobalite)} + 3H_2O \quad (2)$$

Unlike kaolinite which is one of the most used clays in industry, the dehydroxylation of hydroxyl groups in pyrophyllite requires a higher temperature because of the different binding energies in the crystal structure, Table VII [43].

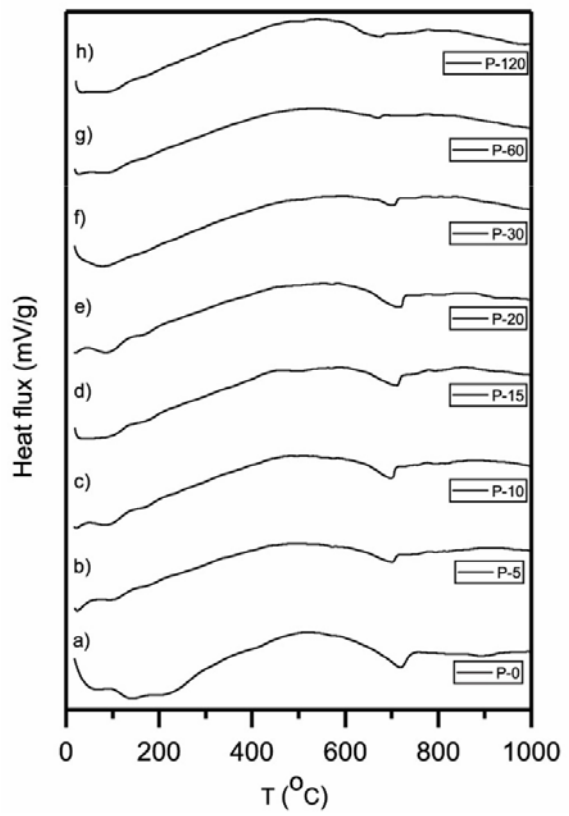

Fig. 8. DTA diagrams before and after milling for different times of pyrophyllite ore from Parsovići, Bosnia and Herzegovina: a) 0 min; b) 5 min; c) 10 min; d) 15 min; e) 20 min; f) 30 min; g) 60 min; h) 120 min.

A large endothermic peak was visible at the DTA curve of the as-received sample, P-0 (Fig. 8), in the temperature range from 590 to 750°C with a maximum at 716°C indicating that the pyrophyllite lost water and that the aluminum-silicate layers separated, resulting in a permanent linear expansion [14, 23]. Since the peak is broad there is also a formation of amorphous SiO_2 taking place in this region as evidenced by FTIR. Due to the reduction of the particle size achieved by mechanochemical treatment, hydroxyl groups are eliminated at lower temperatures. If the milling time is longer, due to the increase in surface energy obtained by milling, the particles become agglomerated and the specific surface area begins to decrease (see Fig. 6). As the milling time becomes longer, these agglomeration processes interfere with the elimination of water caused by heat treatment, and the diffusion of water is hindered [25]. This is also indicated by TG curves that show a reduction in weight loss as milling time increases. The simultaneous loss in the remaining areas of the structural hydroxyl group also declines and is observed at lower temperatures. All these effects are thought to have resulted from the mechanochemical treatment of the base material.

4. Conclusion

The thermal behavior of mechanochemically modified pyrophyllite ore from the Parsovići mine, Bosnia and Herzegovina has been assessed. Morphological and microstructural changes caused by ball milling of pyrophyllite ore for different milling times ranging from 5-120 min with BPR 10 have been followed by XRD, FTIR, SEM-EDS, and particle size analysis. The XRD patterns show a high degree of degradation in comparison to the as-received sample. Delamination, evidenced by FTIR-ATR, a dramatic decrease in particle size (evidenced by PSD) as well as degradation cause partial amorphization of the sample which in turn has influenced the thermal behavior of the material. The SEM-EDS study confirms the change of pyrophyllite ore during mechanical milling. This change is evidenced in particle size diminution and aggregation. As milling time increases, the endothermic DTA peaks associated with dehydroxylation are shifted to lower temperatures. The intensity of dehydroxylation is decreased after 60 min of milling.

Acknowledgments

This paper is supported by the Ministry of Education, Science, and Technological Development of the Republic of Serbia under Grant. No. 451-03-68/2022-14/200017 and the project Proof of concept 5415. The authors are grateful to A.D. HARBI d.o.o Bosnia and Herzegovina for the supply of pyrophyllite ore.

5. References

1. X. Qin, J. Zhao, J. Wang, M. He, Minerals, 10(9) (2020) 778
2. R. Wardle, G. W. Brindley, Am. Mineral., 57 (1972) 732.
3. J. Zhang, J. Yan, J. Sheng, Micron, 71 (2015) 1.
4. I. Tole, K. Habermehl- Cwirzen, A. Cwirzen, Miner. Petrol., 113 (2019) 449.
5. H. Hayashi, K. Koshi, A. Hamada, H. Sakabe, Clay Science, 1 (1962) 99.
6. S. Mohammadnejad, J. L. Provis, J. S. J van Deventer, Hydrometallurgy, 146 (2014) 154.
7. J.L. Pérez-Rodríguez, L. Madrid Sánchez del Villar, P.J. Sánchez-Soto, Clay Miner., 23 (1988) 399.
8. P.J. Sánchez-Soto, A. Justo, J.L. Pérez-Rodríguez, J. Mater. Sci., 29 (1994) 1276.
9. J. M. Filio, K. Sugiyama, F. Saito, Y. Waseda, Int. J. Soc. Mat. Eng. Res., 1(1) (1993) 140 .
10. H. Sayılkan, S. Erdemoğlu, Ş. Şener, F. Sayılkan, M. Akarsu, M. Erdemoğlu, J. Colloid Interf. Sci., 275(2) (2004) 530.
11. J. Temuujin, K. Okada, T. S. Jadambaa, K. J. D.MacKenzie, J. Amarsanaa, J. Eur. Ceram. Soc., 23(8) (2003) 1277.
12. [J. L. Pérez-Rodríguez, A. Wiewiora, V. Ramirez-Valle, A. Durán, L. A. Pérez-Maqueda, J. Phys. Chem. Solids, 68(5-6) (2007) 1225.
13. J. B. Dixon, D. G. Schulze, L. W. Zelazny, P. J. Thomas, C. L. Lawrence, Soil Mineralogy with Environmental Applications, Madison, 2002.
14. T. K. Mukhopadhyay, S. Ghatak, H. S. Maiti, Ceram. Int. 36(3) (2010) 909.
15. G. Li, J. Zeng, J. Luo, M. Liu, T. Jiang, G. Qiu, Appl. Clay Sci., 99 (2014) 282.
16. S. R. Mihajlović, M. M. Vlahović, N. M. Vušović, N. G. Đorđević, M. N. Jovanović, Sci. Sinter., 53(2) (2021) 235.
17. N. Jović-Jovičić, T. Mudrinić, A. Milutinović-Nikolić, P. Branković, Z. Mojović, Sci. Sinter., 53(4) (2021) 535.

18. S. Nenadovic, M. Nenadovic, R. Kovacevic, Lj. Matovic, B. Matovic, Z. Jovanovic, J. Grbovic Novakovic, Sci. Sinter., 41(3) (2009) 309.
19. S. Saxena, M. Prasad, S. S. Amritphale, N. Chandra, Sep. Purif. Technol., 24(1-2) (2001) 263.
20. A. Gücek, S. Şener, S. Bilgen, M. A. Mazmancı, J. Colloid Interf. Sci., 286(1) (2005) 53.
21. Y. Jeong, S. Lee, S. Hong, C. Park, J. Membrane Sci., 536 (2017) 108.
22. R. Ahmad, M. Aslam, E. Park, S. Chang, D. Kwon, J. Kim, Chemosphere 206 (2018) 784.
23. P. Baláž, M. Achimovičová, M. Baláž, P. Billik, Z. Cherkezova-Zheleva, M. J. Criado, F. Delogu, E. Dutková, E. Gaffet, F. J. Gotor, R. Kumar, I. Mitov, T. Rojac, M. Senna, A. Streletskii, K. Wieczorek-Ciurowa, Chem. Soc. Rev., 42(18) (2013) 7571.
24. T. K. Achar, A. Bose, P. Mal, Beilstein J. Org. Chem., 13 (2017) 1907.
25. J. L. P. Rodriguez, P. J. S. Soto, J. Therm. Anal., 37(7) (1991) 1401.
26. K. Sugiyama, J. M. Filio, F. Saito, Y. Waseda, Mineralogical Journal, 17 (1994) 28.
27. P. J. Sánchez-Soto, J. L. Pérez-Rodríguez, I. Sobrados, J. Sanz, Chem. Mater., 9 (1997) 677.
28. P. J. Sánchez-Soto, M. d. C. Jiménez de Haro, L. A. Pérez-Maqueda, I. Varona, J. L. Pérez Rodríguez, J. Am. Ceram. Soc., 83 (2000) 1649.
29. A. Wiewióra, P. J. Sánchez-Soto, M. A. Avilés, A. Justo, J. L. Pérez-Rodríguez, Appl. Clay Sci., 8 (1993) 261.
30. B. -J. Kim, K. H. Cho, B. Chang, H. -S. Kim, S. -G. Lee, C. -Y. Park, S. Lee, N. –C. Choi, Miner. Eng., 140 (2019) 105881.
31. M. Erdemoğlu, M. Birinci, T. Uysal, E. Porgalı Tüzer, T. S. Barry, J. Mater. Sci., 53(19) (2018) 13801.
32. G. K. Williamson, W. H. Hall, Acta Metall. Mater., 1 (1953) 22.
33. R. Hamzaoui, F.; Muslim, S. Guessasma, A. Bennabi, J. Guillin, Powder Technology, 271 (2015) 228.
34. A. Bentayeb, M. Amouric, J. Olives, A. Dekayir, A. Nadiri, Appl. Clay Sci., 22(5) (2003) 211.
35. S. S. Amritphale, S. Bhasin, N. Chandra, Ceram. Int., 32(2) (2006) 181.
36. M. Erdemoğlu, S. Erdemoğlu, F. Sayılkan, M. Akarsu, Ş. Şener, H. Sayılkan, Appl. Clay Sci., 27(1-2) (2004) 41.
37. A. Mitrović, J. Milicević, S. Milošević Govedarović, S. Kurko, T. Pantić, J. Rmuš, J.; Ž. Mravik, J. Grbović Novaković, Pyrophyllite as electrochemical sensors for pesticides, The book of Abstract of Solid-state science and research conference-SCIRES2019, Zagreb, Croatia, June 26-29, 2019. P. 123
38. A. Mitrović, T. Pantić, S. Dimitrijević, A. Ivanović, N. Novaković, S. Kurko, S. Milošević Govedarović, J. Grbović Novaković, Electrochemical sensors based on pyrophyllite, The book of abstract of 14th multinational congress on microscopy-MCM2019, Belgrade, Serbia, Sep 15-20, 2019,p. 494-497
39. J. Milićević, S. Kurko, B. Paskaš Mamula, T. Trtić-Petrović, T. Pantić, S. Milošević Govedarević, A. Hodžić, J. Grbović Novaković, Electrochemical behaviour of pyrophyllite carbon paste composite electrode. Presented at the 2018 3rd International Symposium on Materials for Energy Storage and Conversion, Belgrade, Serbia, Sep 10-12, 2018, p.95
40. Liam R. Wesley, Clays and clay minerals - Geological Origin, Mechanical Properties and Industrial Application;, Nova Science, New York, 2014.
41. V. Balek, L. A. Pérez-Maqueda, J. Poyato, Z. Cerný, V. Ramírez-Valle, I. M. Buntseva, J. L. Pérez-Rodríguez, J. Therm Anal. Cal., 88(1) (2007) 87.
42. V. A. Drits, A. Derkowski, D. K. McCarty, Am. Mineral., 96(1) (2010) 153.

43. R. C. Mackenzie, Differential Thermal Analysis, Academic Press, London, 1970.
44. K. J. D. Mackenzie, I. W. M. Brown, R. H. Meinhold, M. E. Bowden, J. Am. Ceram. Soc., 68(5) (1985) 266.
45. J. J. Fitzgerald, A. I. Hamza, S. F. Dec, C. E. Bronnimann, J. Phys. Chem., 100(43) (1996) 17351.
46. A. Mikuni, C. Wei, R. Komatsu, K. Ikeda, J. Soc. Inor. Mat. Japan, 12 (2005) 191.
47. L. Heller, Am. Mineral. 47(1-2) (1962) 156.
48. G. W. Brindley, R. M. Wardle. Am. Mineral., 55(7-8) (1970) 1259.
49. W. F. Bradley, R. E. Grim, Am. Mineral., 36 (1951) 182.
50. V. P. Ivanova; Termogrammi mineralov. – Zap. Vsesojuz. Min. Obsc., 90: Moskva/Leningrad, Differential Thermal Analysis, Academic Press, London, 1970.
51. G. Kakali, T. Perraki, S. Tsivilis, E. Badogiannis, Appl. Clay Sci., 20 (2001) 73.
52. S. Guggenheim, Y. H. Chang, A. F. Koster van Groos, Am. Mineral. 72 (1987) 537.
53. J. Schomburg, H. Zwahr, J. Therm. Anal., 48 (1997) 135.
54. M. Blasy, Egypt. Int. J. Sc.Eng.Res., 5(2014) 94.
55. F. M. Gonzáles-Miranda, E. Garzon, J. Reca, L. Pérez-Villarejo, S. Martínez-Martínez, P. J. Sánchez-Soto, J. Therm. Anal. Calorim., 132 (2018) 967.

Сажетак: *Ефекат механичког млевења на термичко понашање руде пирофилита са лежишта у Парсовићима, Босна и Херцеговина, окарактерисан је рендгенском дифракцијом праха, инфрацрвеном спектроскопијом Фуријеове трансформације (ФТИР) скенирајућом електронском микроскопијом и дистрибуцијом величине честица. Термичко понашање материјала праћено је термогравиметријском и диференцијалном термичком анализом и повезано је са његовим микроструктурним својствима. Вилиамсон-Хол модел је коришћен за израчунавање величине кристалита и микронапрезања. Механохемијски третман руде пирофилита је довео до значајне структурне модификације, углавном дуж c- осе, што је довело до делимичне деградације кристалне структуре руде. Смањење величине честица, индуковани дефекти и микронапрезање у кристалној решетки узрокују смањење интензитета пика до коначног нестанка. Као што је потврђено скенирајућим електронским микроскопом и анализом расподеле величине честица, специфична површина и агломерација честоца је све израженија како се време млевења повећава. Дехидроксилација минерала се дешава на 716 °C, што је потврђено ФТИР анализом. Ендотермни врх који одговара дехидроксилацији се помера ка нижим температурама и постаје шири, захваљујући формирању аморфног SiO_2 како се време млевења повећава.*
Кључне речи*: термичко понашање, керамички материјали, пирофилит, механохемија, механичко млевење.*